International Journal of Fracture **65:** 345–358, 1994.
© 1994 *Kluwer Academic Publishers. Printed in the Netherlands.*

Crack–particle interaction in two-phase composites Part I: Particle shape effects

P. LIPETZKY and S. SCHMAUDER
Max-Planck-Institut für Metallforschung, Institut für Werkstoffwissenschaft, Seestraße 92, D-70174 Stuttgart, Germany

Received 24 February 1993

Abstract. A plane-strain Finite Element (FE) analysis has been performed on a composite model consisting of a homogeneous, side-cracked elastic material with a single, symmetrically located elastic particle under pure mode-I loading, in an attempt to simply characterize the crack-particle interaction for a general two-phase composite. In order to uniquely characterize the geometry of a given model (crack length, particle size and crack-particle separation) it is necessary to introduce a new comprehensive 'geometric' parameter. For the purpose of making this analysis broadly applicable, a wide range of elastic moduli for both the matrix and the reinforcement are incorporated into the analysis. The results indicate that the particle has a strong influence on the crack-tip stress intensity factor (SIF) only when the particle is relatively *near* the tip as determined by the geometric parameter. Within this crack-tip region it is found that particles elongated parallel to the crack are more able to affect the crack-tip SIF than identically sized particles elongated perpendicular to the crack. Finally, the differential SIF of the composite is given as a general function of the geometric variables, particle shape (aspect ratio) and Dundurs' parameter α which characterizes the elastic mismatch of the constituents. With this relation, a simple and accurate estimate of the elastic interaction between a crack and particles of various shapes can be made on many combinations of materials without an extensive numerical analysis.

1. Introduction

It is increasingly common in new engineering applications to make use of dual-phase composites that combine a matrix material with certain desired properties and a second phase reinforcement with complementary properties, in order to reach better overall performance than is possible for either independent component. One example of this type of composite is the Al-SiC system [1, 2]. The addition of short SiC fibers significantly increases the stiffness, creep resistance and yield strength of aluminum, although much ductility is sacrificed. Implicit in the combination of dissimilar phases are the problems of phase distribution, interfacial bonding, secondary chemical reactions, and misfit stresses. These problems can occasionally be suppressed through altering the chemistry of the composite, or by a subsequent thermal or mechanical treatment. Other examples are metal–metal and ceramic–ceramic composites [3, 4]. All material combinations must overcome these same implicit problems in order to show the maximum mechanical improvement.

This class of new materials has led to the development of models for calculating the effective elastic constants, yield strength and fracture toughness of various combinations of phases in hopes of predicting and optimizing material behavior [5–9]. Restricting ourselves to material fracture leads naturally to the specific problem of a crack in a two-phase material, which has also been addressed in [10–12]. The concensus of composite failure models suggests that the toughness enhancing mechanisms associated with second-phase inclusions are generally twofold: First, inclusions decrease crack growth driving force by deflecting cracks, increasing energy dissipative processes and decreasing stresses ahead of the crack. Simultaneously, the plastic deformation, fracture or interfacial debonding of the second phase in the wake of a crack further increases the energy required for specimen failure [12–14]. Prior to the onset of these mechanisms, cracks must form and extend to the particles. The crack-inclusion inter-

action studies in previous fracture models have generally simplified the composite fracture problem to a system involving only a crack and a circular particle, or a crack and an infinite interface [15]. In order to address the practical material problems more appropriately, it is important to consider not only finite particles with various elastic constants and locations, but also various particle shapes because different processing techniques generate second-phase particles that range from equiaxed to highly elongated. It is known that the interaction between an inclusion and a crack tip is influenced by geometrical factors such as crack length, crack-particle separation and particle size in addition to elastic and thermal misfit stresses, therefore particle shape is one of the remaining important variables which requires investigation.

2. Approach

This work is focussed on the relation between a single particle ahead of a crack tip and the crack-tip stress intensity factor for various crack-particle geometries. The model presented here is intended to characterize the behavior of a crack in the initial stages of composite fracture. A crack in a three-dimensional matrix which encounters fibrous or spherical inclusions behaves differently than any two-dimensional model can predict, although the effects will likely be similar given identical volume fractions in both cases. To directly compare the results of 2-dimensional and 3-dimensional models consider a homogeneous notched specimen loaded in tension. In this case it has been shown that for both elastic and plastic deformation, either a two-dimensional plane-strain or a full three-dimensional analysis can be used to calculate nearly identical stress maxima [16]. As composite cracks are believed to originate largely in the core of specimens, plane strain is chosen over plane stress. Presently, two-dimensional modelling is preferred to three-dimensional in order to simplify the analysis and shorten computation time. Given the fact that the particle nearest the crack tip affects the stress intensity factor directly, the overall volume fraction and distribution of particles are not considered here. Additional distant particles clearly change the overall modulus and stress state but that problem can be roughly analyzed by changing the elastic properties of the matrix to some new 'composite' values [9]. We thus limit ourselves to the elastic interactions in the plane-strain case between a single particle and a crack tip for a side-cracked specimen geometry. This geometry is chosen to maximize the crack-particle interaction effects. A representative schematic of the side-cracked sample geometry is shown in Fig. 1. Characterization of the geometric variables is systematically accomplished through situating cracks of various lengths a fixed distance from an inclusion as shown in Fig. 2, as well as placing a given particle a variable distance from the crack as shown in Fig. 3. The aspect ratio, defined as the dimension of the rectangular particle in the crack plane normalized by the particle height w/h loosely characterizes the shape. The particle aspect ratio as well as the size can then vary for each d and a value. Following this definition, an aspect ratio of 1 applies to a square inclusion, but calculations are also made for a circular particle in order to compare these results with work done by other authors. Aspect ratios here range from $\sim$ 0.05–10 and particle area is $\leq$0.5 percent of the model area.

Mathematical modelling of the mechanical properties of idealized materials is an increasingly important method for interpreting deformation and failure in real materials. Specifically, Finite Element (FE) modelling can be applied to a diverse array of shapes and materials with accurate results. These models can be used to calculate stress, strain and displacement fields as well as energy release rates and stress intensity factors [17]. The PERMAS finite element computer model developed by INTES Corporation is used for the current linear elastic analysis as well as for related elastic-plastic analysis (not reported here) for a more realistic computer

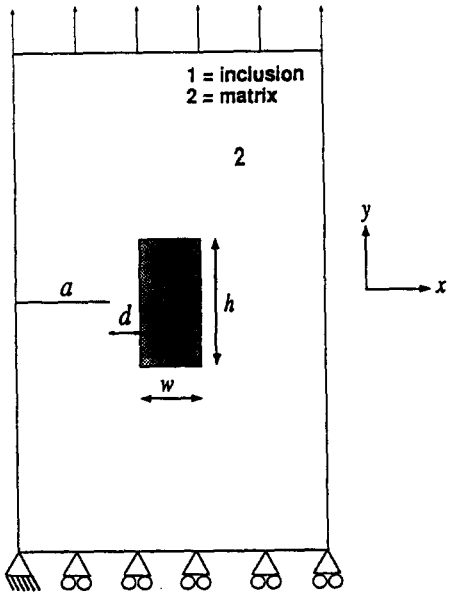

Fig. 1. Schematic of analyzed plane strain model. Particle aspect ratio is defined as the particle width to height ratio w/h.

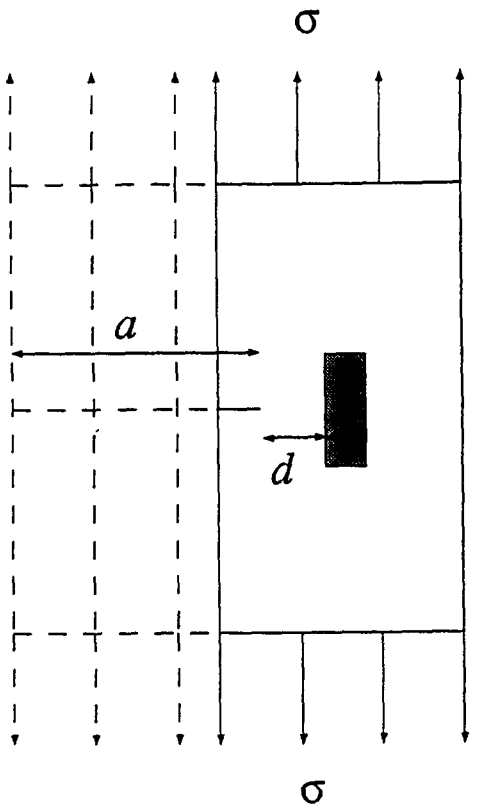

Fig. 2. Variation in a for constant d and far-field stress, σ. Particle volume fraction remains below 0.1 percent.

model [18]. The types of plane-strain elements in use here are both 6-noded triangles, and 8-noded quadrilaterals. Boundary conditions are such that only the upper edge of the specimen is given displacement in the y-direction, less than 0.1percent of the specimen's y dimension, while the vertical faces are stress-free and move without constraint, Fig. 1. Internal stresses and strains arise from the condition that displacements are continuous in the entire model and thus the particle-matrix interface is perfectly bonded. The aspect ratio of the model is approximately 1 : 2 with dimensions a, d, w, $h \leq 10$ percent of the model width. Therefore, the crack-particle interaction can be studied without interference from the horizontal boundary conditions. The specimen is subjected to these displacements, and no thermal or residual stresses are considered at this time. All calculations are based on tensile loading and it is assumed that stresses remain within the elastic range of both the matrix and the inclusion. The specimen was not simplified to one-half its full size because in the course of related calculations some asymmetric features existed in the model [19].

The finite element model described above is used with the modified crack closure integral method to calculate the energy release rate and stress intensity factor at the crack tip [20, 21]. Figure 4 is a reconstruction of the actual crack-tip finite element mesh. The scale of the smallest element at the crack tip is approximately 10 percent of the *minimum* crack length. For clarity the crack location is shown by the line to the left of the expanded area, and all calculations begin with an infinitely sharp crack. The problem is approached by first calculating the nodal point forces near the crack tip. Figure 5 shows the location and origin of such nodal-point

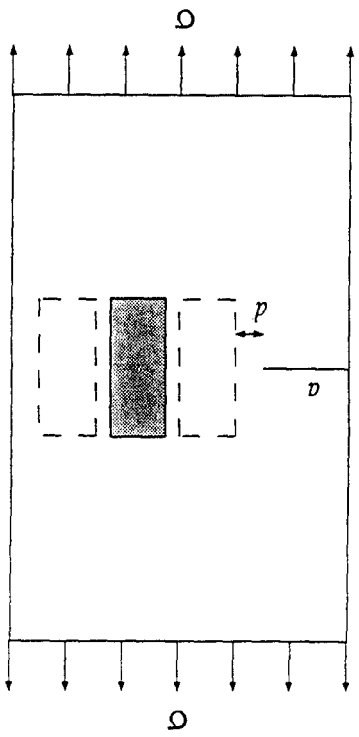

Fig. 3. Constant particle volume fraction for constant far-field stress and a with variable d. Particle size and orientation are unchanged.

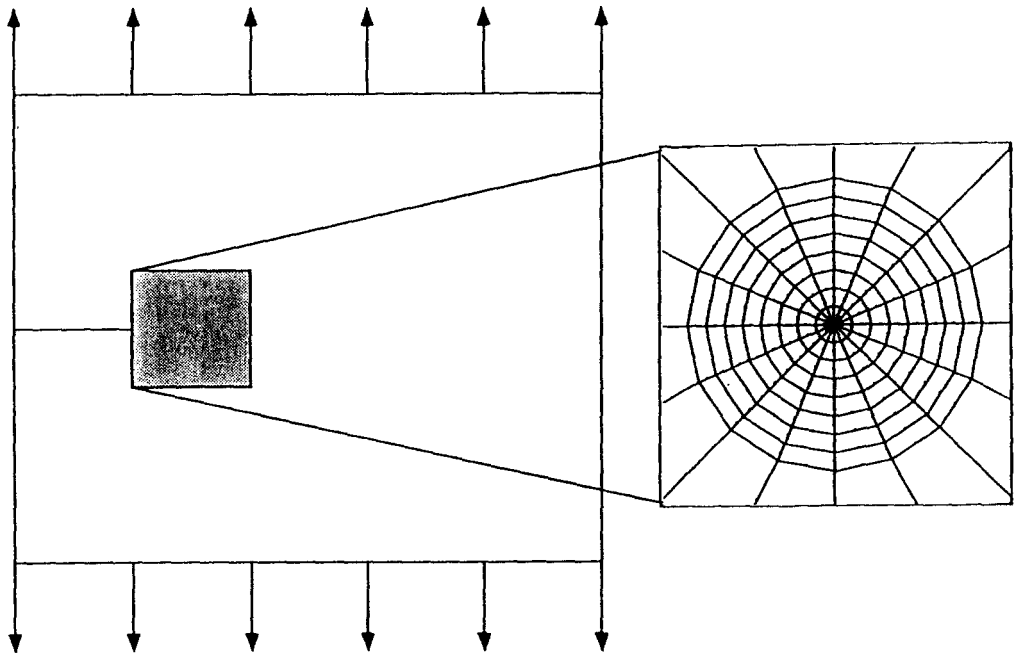

Fig. 4. Symmetric finite element mesh at crack tip.

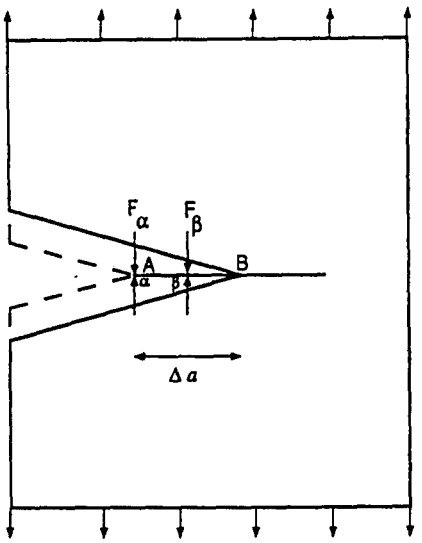

Fig. 5. Selected nodal points and nodal point forces before crack advances to position B. Nodal point forces applied at α and β.

forces. Initially, upper and lower nodes at locations α and β are *attached* by the forces $\mathbf{F}_\alpha$ and $\mathbf{F}_\beta$, thus translate together as the specimen deforms. The nodes are then released from this constraint and the crack propagates a small distance, Δa, from point A to point B. These nodes now have unequal displacement vectors, thus $\Delta \mathbf{u}^\alpha$ and $\Delta \mathbf{u}^\beta$ are no longer zero. The Griffith energy release rate is then calculated as

$$G = \frac{1}{2t\Delta a}[\Sigma F_x \Delta u_x + \Sigma F_y \Delta u_y], \tag{1}$$

where t is the specimen unit thickness, Δa is the incremental crack increase, and $\Sigma F_x \Delta u_x$ is the summation over points α and β of the x-component of the nodal-point forces multiplied by the corresponding displacements. Stress intensity factors are subsequently calculated as

$$K = \sqrt{G\frac{E}{1-\nu^2}}, \tag{2}$$

where E is the stiffness, and ν is Poisson's ratio of the matrix. Stress intensity factors are first calculated for the finite element mesh containing only one material in order to verify a value within 2 percent of the analytical handbook value. The appropriate mesh elements are then assigned the material properties of the inclusion and the calculations are repeated. To insure that this procedure yields correct results, the mesh resolution at both the crack tip and particle-matrix interface is reduced until the K values converge to a constant.

3. Results

The stress intensity factors arising from the FE model for various crack lengths, particle aspect ratios and particle-crack separations are summarized in the following sections. The results are plotted with SIF data on the ordinate and the corresponding crack-particle geometric data on the abscissa. The differential stress intensity, ΔK, is defined as $K_C - K_H$ where K_C is the stress intensity factor of the composite and K_H is the stress intensity factor in the

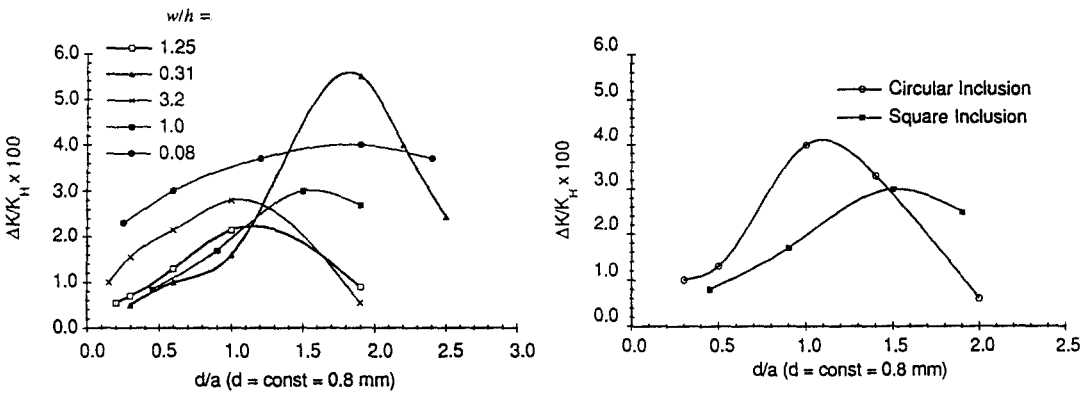

Fig. 6. Results for differential stress intensity factors for (a) rectangular, and (b) square versus circular inclusions. Particles are separated a constant distance d from the crack tip.

homogeneous case. Only the curves for particle aspect ratios 0.08–3.2 are plotted because outside of this range almost no additional changes occurred. The Poisson ratio of 0.3 was used in all reported calculations for both the matrix and inclusion because varying the ν values for both the matrix and inclusion between 0.2 and 0.4 had an insignificant effect on ΔK.

The results of calculations for constant d (0.8 mm) with various particle aspect ratios w/h and crack lengths a for a composite with a hard matrix ($E_m = 210\,\text{GPa}$, $\nu_m = 0.3$) and a soft inclusion ($E_i = 100\,\text{GPa}$, $\nu_i = 0.3$) are plotted on Fig. 6a. The curves exhibit maxima for small values of d/a with $\Delta K/K_H$ values that tend toward zero for more extreme values of d/a. The most extreme peak height corresponds to the aspect ratio 0.31, but is still relatively low at a $\Delta K/K_H$ value near 5 percent. Figure 6b contains a comparison of the results for a circular inclusion and a square inclusion for similar calculations. For both of these inclusions the aspect ratios are equal to one and the areas are equal to $0.8\,\text{mm}^2$, but there are obvious geometrical differences. The same general trends shown for rectangular particles exist for the circular particle, although the peak height for the circular inclusion is roughly double the peak height of the $w/h = 1.25$ rectangle, and 30 percent higher than for the square. The data on Figs. 6a and 6b show that crack length has only a weak influence on ΔK for these values of d and A.

Stress intensity factor-geometry results for the alternate problem involving a variable crack-particle distance and constant crack length are plotted in Fig. 7. The particles retain the same area and aspect ratios as above, while the crack length is kept constant ($a = 0.8\,\text{mm}$) and d is variable. No maximum exists for the data plotted here, rather a monotonic decrease in ordinate values corresponds to an increase in abscissa values for all aspect ratios. For $(d/a) > 1$, the effect of the particle on the differential stress intensity factor diminishes to less than 4 percent of the homogeneous K. The particle begins to have a significant influence only when $(d/a) \leq 1$. For small d, the effects of the particle become large because of the proximity of the inclusion to the crack tip. In this *effective* d/a range (≤ 1) the particle shape effects are strong. For example, at a d/a value of 0.15, the $\Delta K/K_H$ values for the various shapes can range from 17 to 27 percent. Particles elongated parallel to the crack show the greatest SIF enhancement while the circular particle shows the least.

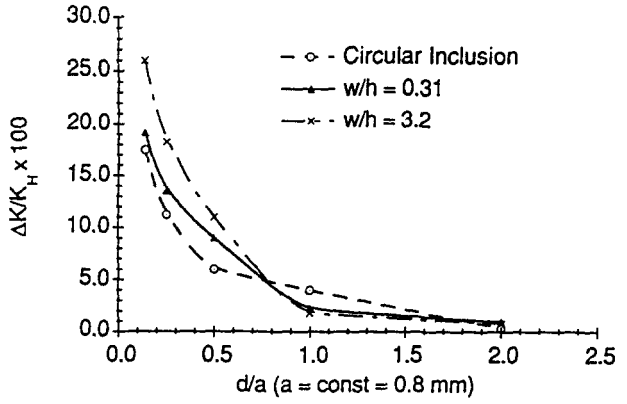

Fig. 7. Influence of crack-particle distance on differential stress intensity factors for two rectangular particles compared to a circular inclusion.

4. Discussion

The interaction between a crack and a particle, as seen in the idealized case above, is influenced by many parameters. The details of actual material failure processes are therefore expected to be hopelessly complex and constantly changing. However, information can be extracted from the current static analysis that facilitates further understanding of the initial stages of deformation and failure in a two-phase composite.

4.1. Geometrical effects

A significant difference in the level of crack-particle interaction exists for not only the different particle aspect ratios, but the variables relating crack size and particle location as well. In Fig. 6 the $\Delta K/K_H$ results for a constant d and variable a are plotted for particles with constant area and various w/h values. The nature of these curves is related to the stress and displacement fields near the crack tip and inclusion. The stress and displacement fields of the crack and particle are comparable in magnitude and in *interactive* contact only for values of $d \approx a$ (≈ 0.8 mm). For more extreme values of d/a, the displacements due to the inclusion and the crack tip are too unevenly matched in magnitude to affect the other to any significant extent. The maximum value of $\Delta K/K_H$ is the point where the interaction is most extensive. It is suggested here without proof that this maximum is related to the interaction between the regions of increased tensile stress that necessarily exist between the crack tip and soft particle. Figure 8 shows the probable expansion and overlap of these regions between the crack and the particle for $d \sim a \sim w$.

Changing the crack-particle geometry variable from a to d reveals that the dominant influence on $\Delta K/K_H$ comes from d. The curves in Fig. 7 approach zero for large values of d/a, although for small d/a values interaction can become as high as 30 percent of the homogeneous SIF. Whereas the curves in Fig. 6 decrease at low d/a values, the data in Fig. 7 continue to increase because the weaker component in close proximity to the crack tip concentrates the stress on the remaining matrix ligament and therefore increases the differential SIF.

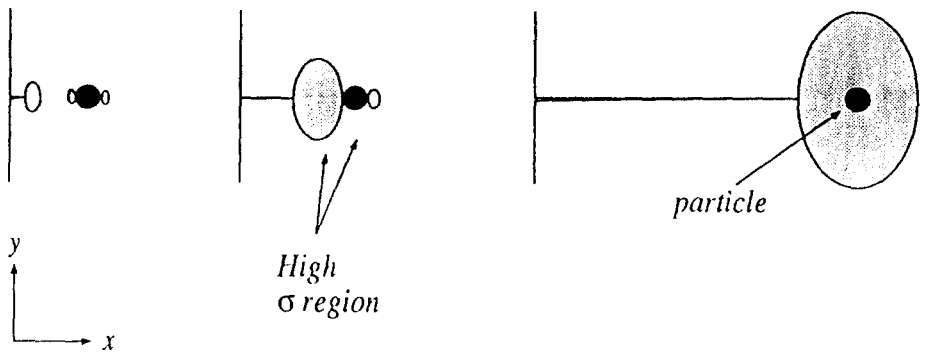

Fig. 8. Schematic showing the stress fields near the crack tip and the inclusion. Shaded regions depict area where $\sigma_{yy} > 2\sigma_{\text{appl}}$ for $a \ll d$, $a = d$, and $a \gg d$.

4.2. Data consolidation

In order to more clearly interpret the crack-particle interaction in a general sense, it is necessary to reconcile the differences between the effects of variable d and variable a. Figures 6 and 7 show that the aspect ratios and d/a ratios can be identical for certain geometries, while the $\Delta K/K_H$ results are different. The magnitudes of a and d must account for this apparent inconsistency. This is not surprising considering that increasing both a and d an order of magnitude for a given particle does not affect the d/a ratio, although a different $\Delta K/K_H$ must result. A new factor is now introduced to the analysis in order to bring the magnitudes of d and a into consideration. This factor arises in an attempt to define the relative scale of the entire problem. Erdogan and others used a factor similar to $a + d + R/a$ for this purpose where R was the circular particle radius, but only considered specific values or combinations of these variables [10, 11]. We attempt to further generalize this factor for a range of values by taking d normalized to a, multiplied by $(d + a)$ normalized to 'R' (here $\sqrt{A}$). This combination now specifies the crack-particle separation relative to the crack length as well as the crack length plus separation relative to the particle size, respectively. Figure 9 contains the previous $\Delta K/K_H$ values for $A = 0.8\,\text{mm}^2$ now plotted as a function of

$$\frac{d}{a}(d + a)\frac{1}{\sqrt{A}}, \tag{3}$$

for abscissa values less than or equal to 3. Three additional data points are also plotted and will be discussed below. The data now show a single trend over the entire abscissa range and the differences between the data are primarily due to the particle aspect ratio. This geometric factor has the advantage of including particle area in $\Delta K/K_H$ calculations as well as the magnitudes of d and a.

The means now exist to express the relationship between the crack driving force $(\Delta K/K_H)$ and the geometric variables of the specimen in a consistent way. The data shown on Fig. 9 roughly follow a parabolic dependence for abscissa values between 0.15 and 1.0. For abscissa values greater than 1.0, ordinate values are a constant $\sim$ 3 percent. Analyzing the data in Fig. 9 indicates that given constant a and A, the influence of a particle on the crack tip decreases as d^2 increases. Conversely for constant d and A, the particle influence can remain small in spite of an increasing a because the abscissa value given by (3) approaches $d/\sqrt{A}$ as a increases. The deviation in the $\Delta K/K_H$ values for a given abscissa value is due to the shape effects. For example, at an abscissa value of 0.28 the different aspect ratio particles yield effects that

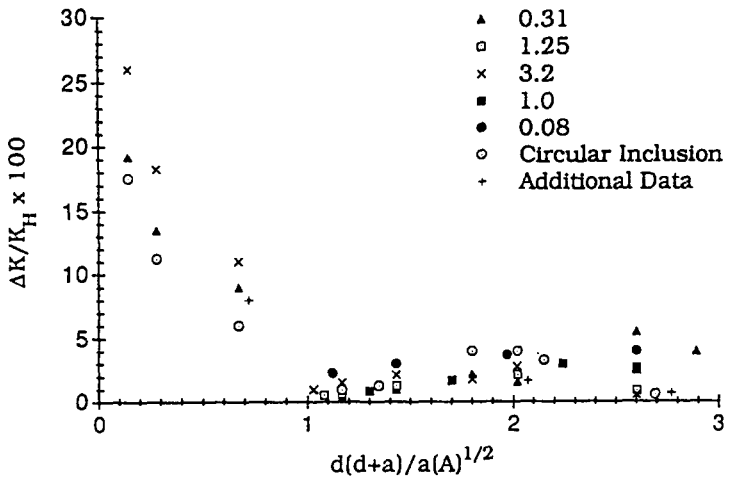

Fig. 9. SIF data for various aspect ratios and crack-particle geometries ($\alpha = -0.35$).

are roughly a factor of 2 different (11–19 percent). A general second-order relation can be written for the various aspect ratio data in the form

$$y = \frac{\Delta K}{K_H} = U\left(\frac{w}{h}\right)x^2 + V\left(\frac{w}{h}\right)x + W\left(\frac{w}{h}\right), \tag{4}$$

for $0.15 \leq x \leq 1.0$. For a range of aspect ratios between 0.31 and 3.2, approximate relations for these coefficients can be written as

$$U\left(\frac{w}{h}\right) = -0.0038\left(\frac{w}{h}\right) + 0.138, \tag{5}$$

$$V\left(\frac{w}{h}\right) = -0.0246\left(\frac{w}{h}\right) - 0.342, \tag{6}$$

and

$$W\left(\frac{w}{h}\right) = 0.0315\left(\frac{w}{h}\right) + 0.219. \tag{7}$$

At the abscissa value of 0.28, the relation here predicts normalized differential stress intensity factors of 21 percent for an aspect ratio of 3 and 14 percent for $w/h = 0.31$.

With the more consistent method of plotting results for different crack-particle geometries and inclusion aspect ratios, it is reasonable to expect that independently changing all of the geometric variables will result in a $\Delta K/K_H$ value that conforms to the current data. For example, with $A = 0.8\,\text{mm}^2$ and $w/h = 1.25$, the previously unused d/a values of 1.5/2.3 and 1.1/1.6 yield values of $\Delta K/K_H = 1$ percent and 1.7 percent for $x = 2.77$, and $x = 2.07$, respectively. These data points show good agreement with the other data plotted in Fig. 9. The d/a values for these two cases are almost identical (0.7) although a necessary separation exists on the abscissa of Fig. 9 because they are clearly two different geometries. Similarly, the d, a and w/h values of 0.8 mm, 1.3 mm and 1.25 respectively, combined with a fourfold increase in particle area ($3.2\,\text{mm}^2$) yields a $\Delta K/K_H$ value of 8 percent for an abscissa value of 0.72. This value is also plotted and shows good agreement with the previous data. With

this consistency now confirmed it is possible to estimate values of $\Delta K/K_H$ for a given d, a and A based either on this data or (4) where

$$x = \frac{d}{a}(d+a)\frac{1}{\sqrt{A}} \leq 1, \tag{8}$$

$0.08 \leq w/h \leq 3.2$ and $U(w/h)$, $V(w/h)$, $W(w/h)$ are given by (5–7). For the similar case of a radial, plane-strain matrix crack in the vicinity of a circular inclusion Mueller et al. have shown analytically that for arbitrary Dundurs' parameters, α and β, the particle effects on the crack tip vary in a manner similar to the data in Fig. 9 [15]. Recall that elastic constant mismatch in two-phase materials is conveniently characterized by the Dundurs' parameters α and β for plane strain as:

$$\alpha = \frac{E_i - E_m}{E_i + E_m}, \tag{9}$$

and

$$\beta = \frac{\alpha}{2}\frac{(1-2\nu)}{(1-\nu)}, \tag{10}$$

where E is the stiffness of the matrix (E_m) and the inclusion (E_i) and ν is the single value of Poisson's ratio for both materials [22]. This comparison will be expanded in Section 4.4.

4.3. Application

With these principles in place, it is now possible to use the results of this model to approximate the level of crack-particle interaction in actual composites. The NiAl-Nb composite is chosen as an example because failure initiates on the NiAl grain boundaries prior to any appreciable plastic deformation [23, 24]. Approximate values for a and d can be taken as roughly one-half of the grain size and one-half of the particle spacing. Particle spacing is necessarily affected by the processing method and the volume fraction. In this composite the Nb volume fraction is kept relatively low (less than 10 percent) in order to retain the favorable high-temperature properties of the matrix as well as the 1 : 1 NiAl stoichiometry. Metallurgical observations of this material reveals that the average grain size for the HIPed NiAl is near 25 μm, although the fluctuation is very large. The average spacing between the 50 μm diameter particles is approximately 200 μm, and the aspect ratios are $\sim$ 1.0–1.5 [25]. Using these approximations for a (10 μm), d (100 μm) and A (2500 μm^2) in (3) indicates that the elastic interaction between the crack and the particle is virtually zero for this configuration. However, due to residual stresses it is more likely that failure will initiate in the regions near the inclusions [26]. Cracks near inclusions would then be strongly attracted to the neighboring particle where plastic energy release may arrest the crack and delay failure thereby stabilizing deformation.

4.4. Generalization

In order to broaden the range of applicability of these findings we now examine other work in an attempt to generalize trends to different combinations of elastic properties. Typical two-phase engineering composites have α and β values that range between $-0.6 < \alpha < 0.6$ and $\beta = \alpha/4 \pm 0.1$ [22, 27]. A comprehensive analysis of the plane-strain elastic interaction between an internal crack and a circular inclusion has yielded the $\Delta K/K_H$ values plotted on

our axis format in Fig. 10 [15]. The curves exhibit low, slowly decreasing values of $\Delta K/K_H$ for abscissa values greater than 1 and roughly a parabolic dependence for abscissa values less than one in a manner similar to that displayed in the current model. The difference between the curves in Fig. 10 is the relative height based on the magnitude of α. The second Dundurs parameter, β, has only a small effect on $\Delta K/K_H$ and will be considered equal to $\frac{1}{4}\alpha$ and otherwise neglected. In an attempt to consolidate the $\Delta K/K_H$ results for various α values, the ordinate format of

$$\frac{-1}{10\alpha}\frac{\Delta K}{K_H} \tag{11}$$

is introduced in Fig. 11. Good agreement exists between all of the data for the range of $-0.6 < \alpha < 0.6$ and $0.14 < x < 2.1$. Fitting these data to a single second-order analytical curve and rewriting gives the relation

$$\frac{\Delta K}{K_H} \approx -10\alpha[H(\alpha)x^2 + K(\alpha)x + L(\alpha)], \tag{12}$$

for x values < 1.2, and for $x > 1.2$,

$$\Delta K/K_H \approx I(\alpha)x + J(\alpha), \tag{13}$$

where

$$H(\alpha) = L(\alpha) = 0.882\alpha^2 - 0.088\alpha + 0.094, \tag{14}$$

$$K(\alpha) = -1.787\alpha^2 + 0.222\alpha - 0.203, \tag{15}$$

and

$$I(\alpha) = 0.00667\alpha - 0.01, \tag{16}$$

$$J(\alpha) = 0.184\alpha^2 - 0.201\alpha + 0.0186, \tag{17}$$

where x is given by (3). Equations (12–17) provide a very simple method for estimating the interaction effects between a circular particle and an internal, radial plane-strain crack in terms of the geometry of the specimen and its relative elastic constants. Mueller's analytical results for the internal crack are fully consistent with the calculations given above for a side-cracked specimen for various inclusion shapes and aspect ratios as shown by the additional data points on Fig. 11.

The results plotted on Fig. 11 show that the elastic parameters of a two-phase system can be included easily into the present analysis. From Section 4.2 above, (4) is given for $\alpha = -0.35$. Utilizing the concepts on Fig. 11 we can now rewrite this equation as

$$\frac{\Delta K}{K_H} \approx -\alpha\left[U'\left(\frac{w}{h}\right)x^2 + V'\left(\frac{w}{h}\right)x + W'\left(\frac{w}{h}\right)\right] \tag{18}$$

where

$$U'\left(\frac{w}{h}\right) = -0.0109\left(\frac{w}{h}\right) + 0.394, \tag{19}$$

$$V'\left(\frac{w}{h}\right) = -0.0703\left(\frac{w}{h}\right) - 0.977, \tag{20}$$

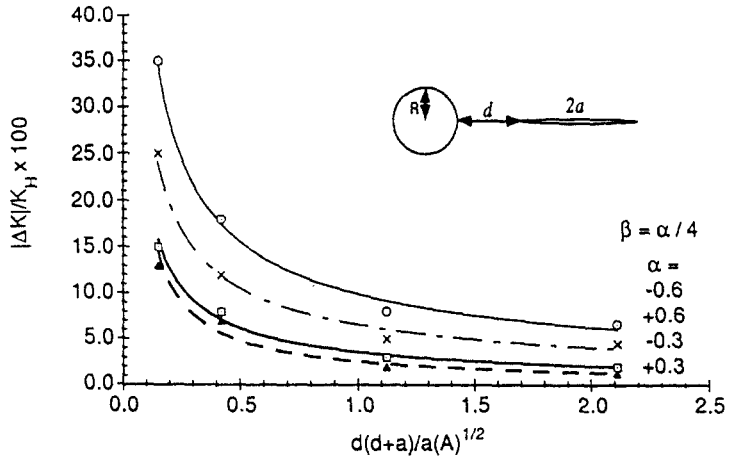

Fig. 10. Summary of the differential stress intensity data for internal radial crack as a function of the elastic constants α and β [15].

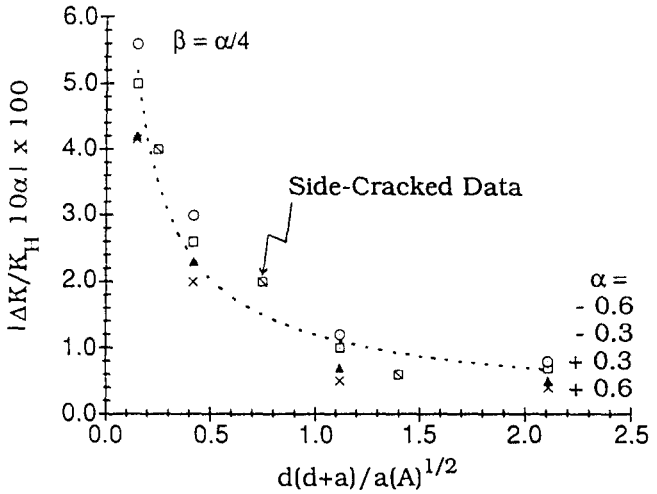

Fig. 11. Normalized stress intensity factors from Fig. 10 replotted on single curve. Additional data points show the comparison between internal and edge-cracked calculations.

and

$$W'\left(\frac{w}{h}\right) = 0.09\left(\frac{w}{h}\right) + 0.626, \tag{21}$$

for abscissa values less than 1 and $0.08 \leq w/h \leq 3$. For values of x between 1 and 5, the simple relation

$$\frac{\Delta K}{K_H} \sim -\frac{\alpha}{10} \tag{22}$$

provides a good approximation for all reasonable α and w/h. This approximation eliminates the necessity of performing a lengthy numerical analysis for general estimates of crack-particle interactions. Perhaps the most important aspect of this result is that predictions of the level of interaction can be made quickly for practically any material combination. As will be shown in Part II of this paper non-symmetric geometries can also be approached in this way with implications for crack deflection and composite toughening.

5. Summary and conclusions

The calculations detailed here show that for a wide range of material combinations and inclusion shapes a good estimate of the elastic crack-particle interaction ($\Delta K/K_H$) can be made by using a simple, closed form relation. The differential crack-tip stress intensity factor is found to vary strongly with crack-particle separation and elastic mismatch, less strongly with particle size and shape, and least strongly with crack length. Specifically, for the most significant elastic interaction between a crack and a symmetrically located particle, the crack tip must be relatively *near* the particle as stated in (8). Resolved in terms of components, (8) implies that

$$d \leq \frac{-a}{2}\left[1 - \sqrt{1 + \frac{4\sqrt{A}}{a}}\right] \tag{23}$$

for a given particle size (A) and crack length (a) in order for elastic interaction effects to be significant. Given this configuration, interaction is proportional to the magnitude of α. Negative α values correspond to an increase in crack driving force and positive α values lead to a decrease in driving force. The remaining variable, aspect ratio, is included in the closed form solutions of (18–21) in the range $0.08 \leq w/h \leq 3.2$. For model geometries corresponding to an abscissa value between 1 and 5, (22) provides a good estimate of $\Delta K/K_H$. These closed form relations are thus powerful tools for estimating the relative strength of the elastic interaction between a crack and a particle given a wide range of specimen geometries and combinations of elastic properties in this symmetric case.

Closer inspection of the effects of particle shape indicates that soft particles elongated parallel to the crack plane attract cracks most strongly because of the enhanced displacements parallel to the loading direction around the particle and at the particle corners. Particles elongated perpendicular to the crack plane are less effective at increasing crack driving force and circular particles are least effective. If the trends shown here for 2-dimensions are followed in a composite, spherical or equiaxed particles will least effectively increase ΔK and thus be the least effective crack attractors. However, following crack-particle intersection, particle shape may take on a very different ranking due to plasticity and debonding.

For inclusions that deform plastically the analysis becomes more complicated due to variable yield stress and strain hardening tendencies. Furthermore, the nonlinear relationship between stress and strain in the plastically deforming particles indicates the $\Delta K/K_H$ curves may display a stronger dependence on the magnitude of crack length and crack-particle separation. Nevertheless, first approximations can be made using this elastic model.

Acknowledgments

Discussions with Dr. A. Wanner regarding the mechanical behavior of NiAl are greatly appreciated. Financial support through the Max-Planck-Gesellschaft and Professor H. Fischmeister is also thankfully acknowledged.

References

1. T. Christman and S. Suresh, *Acta Metallurgica* 36 (1988) 1691–1704.
2. T. Christman, A. Needleman, S. Nutt and S. Suresh, *Materials Science and Engineering* A107 (1989) 49–61.
3. K.K. Chawla, *Composite Materials*, Springer-Verlag, Berlin (1987).

4. E.M. Lenoe, R.N. Katz and J.J. Burke (ed.), *Ceramics for High-Performance Application III, Reliability* (1983).
5. Y.L. Su and J. Gurland, *Materials Science and Engineering* 95 (1987) 151–165.
6. V. Tvergaard, *Acta Metallurgica* 38 (1990) 185–194.
7. F. Erdogan, *Engineering Fracture Mechanics* 4 (1972) 811–840.
8. G. Povirk and A. Needleman, *Journal of Engineering Materials and Technology*, in press.
9. W. Kreher, *ZAMM* 68 (1988) 147–154.
10. F. Erdogan, G.D. Gupta and M. Ratwani, *Journal of Applied Mechanics* (1974) 1007–1013.
11. W. Mueller and S. Schmauder, *International Journal of Solids and Structures* 29 (1992) 1907–1918.
12. T. Faber and A.G. Evans, *Journal of the American Ceramic Society* (1989) Parts I and II.
13. M.F. Ashby, F.J. Blunt and M. Bannister, *Acta Metallurgica* 37 (1989) 1847–1855.
14. M.C. Shaw, D.B. Marshall and A.G. Evans, in *Proceedings, Material Research Society Symposium* 170 (1990) 25–39.
15. W. Mueller, S. Schmauder, A.G. Evans and R.M. McMeeking, *International Journal of Fracture*, in press.
16. R. Twickler, M. Twickler and W. Dahl, *Engineering Fracture Mechanics* 24 (1986) 553–565.
17. O.C. Zienkiewicz, *The Finite Element Method in Engineering Science*, McGraw-Hill, London (1971).
18. INTES Corp., Industriestr. 2, D-7000 Stuttgart 80.
19. P. Lipetzky and S. Schmauder, Crack–Particle Interaction in Two-Phase Composites: Part II, Crack Deflection, *International Journal of Fracture*, submitted.
20. F.G. Buchholz and M.F. Kanninen, *Paper presented at First World Congress on Computational Mechanics*, (WCCM1), Austin, Texas, USA (1986).
21. E.F. Rybicki and M.F. Kanninen, *Engineeering Fracture Mechanics* 9 (1977) 931–938.
22. S. Schmauder and M. Meyer, *Z Metallkd* 83 (1992) 524–527.
23. K.H. Hahn and K. Vedula, *Scripta Metallurgica* 23 (1989) 7–12.
24. A.G. Rozner and R.J. Wasilewski, *Journal of Inst Met* 94 (1966) 169–175.
25. Personal communication, Dr. A. Wanner, MPI, Stuttgart.
26. P. Lipetzky, A. Wanner and B. Schietinger, manuscript in preparation.
27. T. Suga, G. Elssner and S. Schmauder, *Journal of Composite Materials* 22 (1988) 917–921.